RESEARCH ARTICLE

Synthesis and Characterization of Curcumin Analogues with Enhanced Antidiabetic, Anti-Inflammatory, and Anticancer Activity

Pooja G. Swami[1], Rajkumar S Bagali[2], Ashok Sarjerao Narute[3], Jenish Bhagat[4], Nidhi Pathak[5], Swati Madan[6], Shikha Saxena[6] and Ramanpreet Walia[6]*

[1]Institute of Pharmaceutical Education and Research, Borgaon (Meghe), Wardha.

[2]Annasaheb Dange College of B Pharmacy, Ashta Maharashtra 416301.

[3]Yash Institute of Pharmacy, South City, Waluj Road, Tisgaon, Chhatrapati Sambhajinagar, Maharashtra -431136.

[4]Department of Pharamaceutics,Parul Institute of Pharmaceutical Education and Research,Faculty of Pharmacy,Parul University,Vadodara,Gujarat

[5]Department of Chemistry, Faculty of Science and Humanities, SRM Institute of Science and Technology, Delhi-NCR Campus, Modinagar, Ghaziabad, Uttar Pradesh, 201204, India.

[6]Amity Institute of Pharmacy, Amity University, Amity Rd, Sector 125, Uttar Pradesh 201301. Noida.

***Corresponding Author:**

Dr. Ramanpreet Walia,

Professor,

Amity Institute of Pharmacy, Amity University, Amity Rd, Sector 125, Uttar Pradesh 201301. Noida.

E mail: rwalia@amity.edu

Abstract

Curcumin (1,7-bis(4-hydroxy-3-methoxyphenyl)-1,6-heptadiene-3,5-dione), a polyphenolic phytoconstituent derived from the rhizomes of Curcuma longa Linn., has long been recognized as a pharmacologically versatile scaffold exhibiting antidiabetic, anti-inflammatory, anticancer, and antioxidant properties. Despite its broad therapeutic potential, the clinical translation of curcumin has been severely hampered by its inherent physicochemical limitations, including extremely poor aqueous solubility (11 ng/mL at physiological pH), rapid metabolic conjugation, photodegradation, and limited systemic bioavailability. To overcome these shortcomings and augment pharmacological efficacy, a series of eight structurally diverse curcumin analogues (CA-1 through CA-8) was designed, synthesized, and comprehensively characterized in the present investigation. The synthetic strategy involved Claisen–Schmidt condensation of substituted aldehydes with acetylacetone or its congeners, followed by selective Knoevenagel condensation, O-alkylation, and ester bioisostere incorporation as warranted by the structural target. All synthesized compounds were purified by column chromatography and recrystallization, and characterized by UV-Vis, FTIR, ^{1}H-NMR, ^{13}C-NMR, and high-resolution mass spectrometry (HRMS). The compounds were evaluated for in vitro antidiabetic activity (α-amylase and α-glucosidase inhibition), anti-inflammatory activity (albumin denaturation inhibition and COX-2 inhibitory assay), and anticancer activity (MTT assay on MCF-7 breast cancer and HeLa cervical carcinoma cell lines). Molecular docking studies against PDB targets 3L4W (α-glucosidase), 1EQG (COX-2), and 3ERT (estrogen receptor-α) corroborated the in vitro findings. ADME profiling using SwissADME and pkCSM platforms confirmed drug-likeness of selected analogues. Among the analogues, CA-3 (3,4-dimethoxy-substituted) and CA-7 (fluorinated aryl congener) demonstrated the most potent multitarget activity with IC_{50} values superior to curcumin and comparable to reference standards. The study establishes a rational structure–activity relationship framework and identifies CA-3 and CA-7 as promising lead candidates warranting further pre-formulation and pharmacokinetic investigation.

Keywords: Curcumin analogues; antidiabetic activity; anti-inflammatory; anticancer; MTT assay; molecular docking; structure–activity relationship; ADME prediction; α-glucosidase inhibition; Claisen–Schmidt condensation.

How to cite this article: Swami PG, Bagali RS, Narute AS, Bhagat J, Pathak N, Madan S, Saxena S, Walia R. Synthesis and Characterization of Curcumin Analogues with Enhanced Antidiabetic, Anti-Inflammatory, and Anticancer Activity. Int J Drug Deliv Technol. 2026;16(23s): 191-203. DOI: 10.25258/ijddt.16.23s.23

Introduction

The global burden of non-communicable diseases (NCDs) including type 2 diabetes mellitus (T2DM), chronic inflammation, and cancer has reached unprecedented proportions in the twenty-first century. According to the International Diabetes Federation, approximately 537 million adults worldwide lived with diabetes in 2021, a figure projected to surpass 780 million by 2045.[1] Cancer, on the other hand, remains the second leading cause of mortality globally, with an estimated 19.3 million new cases reported in 2020 alone.[2] Chronic, low-grade inflammation is now widely recognized as a molecular nexus connecting T2DM and cancer

pathogenesis, reinforcing the urgent need for multitarget therapeutic agents capable of simultaneously modulating metabolic and inflammatory pathways.[3]

Curcumin (diferuloylmethane), the principal bioactive curcuminoid of Curcuma longa L. (family Zingiberaceae), has attracted exceptional scientific attention owing to its remarkable polypharmacological profile. Accumulated evidence from over four decades of research attests to its potent antioxidant, anti-inflammatory, immunomodulatory, antidiabetic, and anticancer activities.[4] The mechanistic basis of curcumin's anti-inflammatory action involves the inhibition of NF-κB, cyclooxygenase-2 (COX-2), lipoxygenase-5, and inducible nitric oxide synthase (iNOS), thereby suppressing the biosynthesis of pro-inflammatory prostaglandins, leukotrienes, and reactive nitrogen intermediates.[5] Its antidiabetic mechanism is mediated through α-glucosidase and α-amylase inhibition—enzymes that govern postprandial glucose absorption—as well as through PPAR-γ agonism, AMPK activation, and insulin secretagogue effects on pancreatic β-cells.[6] In the oncological domain, curcumin exerts pleiotropic effects encompassing induction of apoptosis via Bcl-2/Bax modulation, suppression of VEGF-mediated angiogenesis, inhibition of Akt/mTOR signaling, and downregulation of cyclin D1-dependent cell cycle progression.[7]

Despite this expansive pharmacological repertoire, curcumin's clinical utility is fundamentally constrained by its unfavorable biopharmaceutical profile. The compound is characterized by extremely low aqueous solubility (11 ng/mL), high lipophilicity (log P ≈ 3.29), rapid intestinal and hepatic metabolism involving phase II glucuronidation and sulfation, susceptibility to alkaline hydrolysis and photodegradation, and a systemic bioavailability of less than 1% following oral administration.[8] These limitations have prompted researchers to explore diverse strategies for circumventing curcumin's physicochemical shortcomings, including nanoparticulate delivery systems, prodrug strategies, and structural modification through medicinal chemistry.

Structural modification of curcumin through rational analogue design has emerged as one of the most productive avenues in curcumin-based drug discovery. The β-diketone moiety, which confers pharmacological activity but is also largely responsible for metabolic instability, has been a primary focus of synthetic intervention.[9] Replacement of the β-diketone with pyrazole, isoxazole, or boronate bioisosteres, methylenation of phenolic hydroxyls, introduction of halogen atoms at the arene ring, and strategic placement of electron-donating or electron-withdrawing substituents have all been reported to modulate the in vitro pharmacological profile, metabolic stability, and solubility of curcumin analogues.[10] Notably, monocarbonyl analogues of curcumin (MACs) have attracted considerable interest as they lack the reactive β-diketone tautomer and consequently exhibit superior metabolic resistance while retaining or augmenting anti-inflammatory and anticancer potency.[11]

Several structure–activity relationship (SAR) studies have established that electron-donating substituents (methoxy, hydroxyl) at the para position of the aryl rings and halogens (fluorine, chlorine) at the ortho or meta positions substantially enhance binding affinity toward COX-2, α-glucosidase, and estrogen receptor-α.[12] Fluorinated curcumin analogues have demonstrated particularly promising anti-inflammatory and antiproliferative profiles, attributed to improved metabolic stability of the C–F bond and enhanced hydrophobic interactions within enzyme active sites.[13] Similarly, methoxy-substituted analogues have been shown to exhibit superior α-glucosidase inhibitory activity compared to parent curcumin, with IC_{50} values in the sub-micromolar range, substantially outperforming the clinical reference acarbose.[1′]

In the present study, we report the design, synthesis, and comprehensive in vitro and in silico evaluation of eight novel curcumin analogues incorporating diverse aromatic substituents including methoxy, dimethoxy, fluorine, chlorine, hydroxyl, and nitro groups. The synthetic approach employed Claisen–Schmidt condensation and Knoevenagel condensation as the primary bond-forming strategies, reflecting an operationally simple, atom-economical route amenable to structural diversification. The analogues were subjected to systematic spectroscopic characterization, physicochemical profiling, and biological evaluation for antidiabetic, anti-inflammatory, and anticancer activities. Molecular docking and ADME analyses provided mechanistic rationalization of the observed biological data and confirmed the drug-likeness of the most active candidates. This study contributes a coherent SAR framework to the growing body of curcumin medicinal chemistry literature and identifies CA-3 and CA-7 as high-priority lead compounds for further pharmacological development.

Materials

All chemicals, reagents, and solvents employed in the present study were of analytical reagent (AR) grade and were procured from established commercial suppliers. Curcumin (purity ≥98%, HPLC-grade) was obtained from Sigma-Aldrich (St. Louis, MO, USA). Aromatic aldehydes including 4-hydroxybenzaldehyde, 4-methoxybenzaldehyde, 3,4-dimethoxybenzaldehyde, 4-fluorobenzaldehyde, 4-chlorobenzaldehyde, 2-hydroxybenzaldehyde (salicylaldehyde), 4-nitrobenzaldehyde, and 3,4-methylenedioxybenzaldehyde (piperonal) were sourced from TCI Chemicals (Tokyo, Japan) and Merck Life Science (Mumbai, India). Acetylacetone (2,4-pentanedione), benzoylacetone, malononitrile, ethyl cyanoacetate, piperidine,

glacial acetic acid, boron trifluoride diethyl etherate ($BF_3 \cdot OEt_2$), anhydrous potassium carbonate, dimethyl sulfoxide (DMSO), methanol, ethanol, chloroform, ethyl acetate, petroleum ether (60–80°C), and n-hexane were procured from Loba Chemie Pvt. Ltd. (Mumbai, India) and S.D. Fine Chemicals (Mumbai, India). Silica gel 60 (mesh 70–230, for column chromatography) and silica gel 60 F_{254} pre-coated aluminum sheets (for thin-layer chromatography, TLC) were obtained from Merck (Darmstadt, Germany). For biological assays, α-amylase from porcine pancreas (EC 3.2.1.1, 17 U/mg), α-glucosidase from Saccharomyces cerevisiae (EC 3.2.1.20, ≥10 U/mg), bovine serum albumin (BSA, Fraction V, ≥98%), p-nitrophenyl-α-D-glucopyranoside (pNPG), 3-(4,5-dimethylthiazol-2-yl)-2,5-diphenyltetrazolium bromide (MTT), dimethyl sulfoxide (cell-culture grade), and 3,5-dinitrosalicylic acid (DNS) were procured from Sigma-Aldrich. The COX Inhibitor Screening Assay Kit (Colorimetric, Item No. 560131) was obtained from Cayman Chemical (Ann Arbor, MI, USA). Acarbose, indomethacin, and doxorubicin were used as reference standards and were procured from a certified pharmaceutical supplier. Human breast adenocarcinoma cells (MCF-7) and human cervical carcinoma cells (HeLa) were obtained from the National Centre for Cell Science (NCCS), Pune, India, and were maintained in Dulbecco's Modified Eagle's Medium (DMEM, HiMedia, Mumbai) supplemented with 10% fetal bovine serum (FBS), 100 U/mL penicillin, and 100 µg/mL streptomycin at 37°C under 5% CO_2. All analytical measurements were performed using calibrated and validated instrumentation, including a Shimadzu UV-2600 UV-Vis spectrophotometer, a PerkinElmer Spectrum Two FTIR spectrometer (KBr disc method), a Bruker Avance III HD 400 MHz NMR spectrometer ($CDCl_3$ or DMSO-d_6 as solvent, TMS as internal standard), and a Bruker MicrOTOF-Q II high-resolution mass spectrometer (ESI mode). Melting points were determined on a Buchi M-565 digital melting point apparatus and are uncorrected.

Methods

General synthetic strategy

The synthesis of curcumin analogues was accomplished primarily through Claisen–Schmidt condensation and Knoevenagel condensation protocols, both of which are characterized by mild reaction conditions, high atom economy, and excellent functional group tolerance. The general synthetic design involved the aldol-type condensation of appropriately substituted aromatic aldehydes with active methylene compounds (acetylacetone, benzoylacetone, malononitrile, or ethyl cyanoacetate) under basic or acidic catalysis. The β-diketone-containing analogues (CA-1 to CA-5) were obtained via Claisen–Schmidt condensation, while the cyanoacetate- and malononitrile-based analogues (CA-6, CA-7) were prepared through Knoevenagel condensation. A boron-chelated analogue (CA-8) was prepared from the best-performing β-diketone precursor using $BF_3 \cdot OEt_2$. Reaction progress was monitored by TLC using silica gel F_{254} plates with UV visualization (254 and 365 nm) and 5% ethanolic iodine solution as a general stain. All reactions were conducted under solvent-optimized conditions in round-bottom flasks equipped with a magnetic stirrer and a reflux condenser. Completion was confirmed when a single spot was observed corresponding to the product, with disappearance of aldehyde starting material.

Synthesis of Curcumin Analogues (CA-1 to CA-5): Claisen–Schmidt Condensation

The general procedure for synthesis of β-diketone analogues is described herein. In a representative synthesis, acetylacetone (2.0 mmol, 200 mg) was dissolved in 15 mL of absolute ethanol in a 100 mL round-bottom flask. The appropriate aromatic aldehyde (4.4 mmol, 2.2 equivalents) was added, followed by piperidine (0.2 mmol, 20 µL, 10 mol%) as the base catalyst and glacial acetic acid (0.2 mmol, 12 µL) as an activating co-catalyst. The reaction mixture was heated to 60°C with constant magnetic stirring and maintained at reflux for 4–8 hours, depending on the electrophilicity of the aldehyde. Upon reaction completion as confirmed by TLC, the mixture was cooled to room temperature and poured into 50 mL of ice-cold water with stirring, inducing precipitation of the crude product. The precipitate was collected by vacuum filtration, washed successively with cold water (3 × 10 mL) and cold ethanol (2 × 5 mL) to remove unreacted starting materials, and air-dried at 45°C for 12 hours. For CA-1, benzaldehyde (unsubstituted, reference analogue) was employed; CA-2 used 4-methoxybenzaldehyde; CA-3 used 3,4-dimethoxybenzaldehyde; CA-4 used 4-chlorobenzaldehyde; and CA-5 used 2-hydroxybenzaldehyde. Yields ranged from 58–82% depending on substituent electronics and steric considerations.

Synthesis of CA-6 and CA-7: Knoevenagel Condensation

Knoevenagel condensation was employed for the synthesis of CA-6 (ethyl cyanoacetate-based) and CA-7 (malononitrile-based, fluorinated aryl). For CA-6, 4-hydroxybenzaldehyde (2.0 mmol, 244 mg) and ethyl cyanoacetate (2.0 mmol, 226 mg) were dissolved in a mixture of ethanol–water (4:1, v/v, 20 mL). Piperidine (0.3 mmol, 30 µL, 15 mol%) was added dropwise with stirring at ambient temperature. The reaction was stirred at 50°C for 6 hours, after which the solvent was evaporated under reduced pressure. The residue was dissolved in ethyl acetate (30 mL), washed with 1 N HCl (2 × 10 mL) and brine (10 mL), dried over anhydrous Na_2SO_4, and concentrated in vacuo. The crude product was purified by silica gel column chromatography (see Section 3.5). CA-7 was synthesized from 4-fluorobenzaldehyde (2.0 mmol, 248 mg)

and malononitrile (2.0 mmol, 132 mg) in ethanol (15 mL) with piperidine catalysis (0.2 mmol) at 40°C for 3 hours; the short reaction time reflects the superior nucleophilicity of malononitrile and the electron-withdrawing effect of fluorine.

Synthesis of CA-8: Boron-Chelated Curcumin Analogue

The boron-chelated analogue CA-8 was prepared from CA-3 (3,4-dimethoxy-substituted β-diketone analogue) as a one-step complexation. CA-3 (1.0 mmol, approx. 356 mg) was dissolved in dry acetonitrile (15 mL) in a flame-dried two-neck flask under nitrogen atmosphere. Boron trifluoride diethyl etherate ($BF_3 \cdot OEt_2$, 1.1 equivalents, 139 mg) was added dropwise via a syringe at 0°C, and the reaction was warmed to room temperature and stirred for 2 hours. The resulting orange-red precipitate was filtered, washed with diethyl ether (3 × 10 mL), and dried under vacuum at 40°C. Boron chelation was confirmed by the characteristic shift in the FTIR carbonyl stretching frequency and the disappearance of the enol O–H stretch, along with a diagnostic downfield shift in the ^{1}H-NMR spectrum and a molecular ion consistent with a 1:1 boron-to-ligand complex in the HRMS spectrum.

Purification Techniques

All synthesized analogues were purified using two sequential approaches: preliminary purification by recrystallization from suitable solvent systems, followed by column chromatographic purification of analogues that failed to yield analytically pure material by recrystallization alone. For recrystallization, the crude solid was dissolved in a minimum volume of hot ethanol, filtered while hot to remove insoluble impurities, and the filtrate was allowed to cool slowly at 4°C. The resulting crystals were collected by filtration, washed with cold ethanol, and dried. Column chromatography was performed on silica gel 60 (230–400 mesh) packed as slurry in petroleum ether. Gradient elution was employed with increasing proportions of ethyl acetate in petroleum ether (5–40% EtOAc/hexane), and fractions of 10 mL were collected and analyzed by TLC. Fractions containing the pure product (single spot, identical R^f value) were pooled and concentrated under reduced pressure. Purity of all final compounds (≥98%) was confirmed by HPLC analysis (C18 reverse-phase column, acetonitrile–water gradient, UV detection at 420 nm).

Spectroscopic Characterization

UV-Vis absorption spectra of all analogues (10 μM in methanol or DMSO) were recorded on a Shimadzu UV-2600 spectrophotometer in the range 200–700 nm. Curcumin analogues characteristically exhibit dual absorption bands: a π–π* transition in the range 260–290 nm attributable to the phenyl chromophore and an extended n–π* or charge-transfer band in the range 380–430 nm associated with the conjugated enone system. Spectral shifts relative to parent curcumin (λmax 429 nm in methanol) were interpreted in the context of the electronic effect of ring substituents.

FTIR spectra were recorded as KBr pellets on a PerkinElmer Spectrum Two spectrometer over the range 4000–400 cm^{-1}. Key absorption bands were assigned and interpreted: broad O–H stretch (3200–3500 cm^{-1}, phenolic and enolic hydroxyl), C–H stretch (2850–2960 cm^{-1}, aromatic and aliphatic), conjugated C=O stretch (1620–1650 cm^{-1}, shifted to lower wavenumber relative to unconjugated ketone due to extended conjugation), C=C stretch (1560–1600 cm^{-1}), and C–O–C stretch (1030–1250 cm^{-1}, methoxy and ether groups).

^{1}H-NMR and ^{13}C-NMR spectra were recorded in deuterated DMSO-d_6 or $CDCl_3$ on a Bruker Avance III HD 400 MHz NMR spectrometer. Chemical shifts (δ) are reported in parts per million (ppm) referenced to TMS (0.00 ppm for ^{1}H) or the residual solvent signal. Multiplicities are denoted as s (singlet), d (doublet), dd (doublet of doublets), t (triplet), and m (multiplet), and coupling constants (J) are given in Hz. The α,β-unsaturated protons H-α and H-β of the enone system typically appear as doublets in the range δ 6.50–7.60 ppm with a characteristic large trans coupling constant (J = 15–16 Hz), confirming E-configuration of the double bond. The methylene proton (H_3 of the diketone central carbon) appears as a singlet around δ 6.00–6.20 ppm in non-chelated analogues, while it is absent in the boron-chelated analogue (CA-8). Aromatic protons resonate in the range δ 6.80–8.30 ppm, and methoxy groups appear as singlets at δ 3.80–3.95 ppm.

High-resolution mass spectra (HRMS) were acquired in positive electrospray ionization (ESI+) mode on a Bruker MicrOTOF-Q II mass spectrometer. Molecular formulae were assigned based on $[M+H]^+$ ions with mass accuracy within ±5 ppm. Isotope pattern matching further confirmed the proposed structures.

Physicochemical Evaluation

Aqueous solubility of each analogue was determined by the miniaturized shake-flask method. An excess amount of each compound was added to phosphate-buffered saline (PBS, pH 7.4) in a 1.5 mL microcentrifuge tube and vortexed for 5 minutes, followed by incubation at 37°C with orbital shaking at 150 rpm for 24 hours. The suspension was filtered through a 0.45 μm PTFE membrane filter, and the filtrate was quantified by UV spectrophotometry at the compound's characteristic λmax. All measurements were performed in triplicate (n=3) and reported as mean ± standard deviation (μg/mL). Stability studies were conducted in PBS (pH 7.4) and simulated intestinal fluid (SIF, pH 6.8) at 37°C over 72 hours. Aliquots were withdrawn at 0, 1, 2, 4, 8, 24, 48, and 72 hours, filtered, and analyzed by HPLC to determine the percentage of intact compound remaining. Photostability was assessed by exposing methanolic solutions (10 μM) to UV light (365 nm) for 6 hours and monitoring absorbance changes.

***In Vitro* Antidiabetic Assays**

Alpha-amylase inhibitory activity was determined by the 3,5-dinitrosalicylic acid (DNS) colorimetric method. In a 1.5 mL tube, 50 µL of each test compound (dissolved in DMSO and diluted to yield concentrations of 3.125–200 µg/mL in PBS, final DMSO ≤1%) was mixed with 50 µL of porcine pancreatic α-amylase solution (2 U/mL in 20 mM sodium phosphate buffer, pH 6.9, containing 6 mM NaCl). The mixture was pre-incubated at 37°C for 10 minutes, and then 100 µL of 1% starch substrate solution was added. After exactly 15 minutes of incubation at 37°C, the reaction was terminated by the addition of 200 µL of DNS reagent. The tubes were heated in a boiling water bath for 5 minutes, cooled, and the absorbance was measured at 540 nm using a microplate reader. Acarbose was used as the positive control. IC_{50} values were calculated from dose-response curves using GraphPad Prism 9.0 (four-parameter logistic model).

Alpha-glucosidase inhibitory activity was evaluated using p-nitrophenyl-α-D-glucopyranoside (pNPG) as substrate. Briefly, 50 µL of each test compound (1.5625–100 µg/mL) was incubated with 50 µL of α-glucosidase (0.5 U/mL in 0.1 M sodium phosphate buffer, pH 6.8) at 37°C for 10 minutes. The enzyme reaction was initiated by the addition of 50 µL of 5 mM pNPG substrate, and the mixture was incubated for 30 minutes at 37°C. The reaction was stopped by addition of 100 µL of 0.1 M sodium carbonate solution. Liberation of p-nitrophenol was quantified by measuring absorbance at 405 nm. The percentage inhibition was calculated as: % inhibition = [(Ac – As)/Ac] × 100, where Ac is the absorbance of control (enzyme + substrate, no inhibitor) and As is the absorbance of test sample. Acarbose served as the reference inhibitor.

***In Vitro* Anti-inflammatory Assays**

Protein (albumin) denaturation inhibition assay was employed as a primary screen for anti-inflammatory activity. The test solution (2 mL) comprised 0.45 mL of 5% w/v BSA in PBS (pH 6.4) and 2.8 mL of test compound at concentrations ranging from 31.25 to 500 µg/mL. The pH was adjusted to 6.4 using 1 N HCl. The mixture was incubated at 37°C for 20 minutes and subsequently subjected to thermal denaturation at 57°C for 30 minutes in a water bath. After cooling, turbidity was measured at 660 nm. Indomethacin was used as the standard reference (0.1–50 µg/mL). The percentage inhibition of protein denaturation was calculated, and IC_{50} values were determined by non-linear regression analysis.

COX-2 inhibitory activity was determined using the Cayman Chemical COX Inhibitor Screening Assay Kit (colorimetric format, Item No. 560131), which employs the peroxidase component of COX to oxidize a chromogenic substrate (N,N,N',N'-tetramethyl-p-phenylenediamine, TMPD) in the presence of arachidonic acid. Briefly, test compounds were added to the reaction mixture containing ovine COX-2 enzyme and pre-incubated at room temperature for 5 minutes. Arachidonic acid (100 µM) was then added to initiate the reaction, and the colorimetric change was measured at 590 nm after 5 minutes. Celecoxib was included as a selective COX-2 reference inhibitor.

***In Vitro* Anticancer Activity: MTT Assay**

The antiproliferative activity of synthesized analogues was evaluated against MCF-7 (human breast adenocarcinoma) and HeLa (human cervical carcinoma) cell lines using the MTT [3-(4,5-dimethylthiazol-2-yl)-2,5-diphenyltetrazolium bromide] colorimetric assay. Cells were seeded in 96-well flat-bottom plates at a density of 5×10^3 cells/well (MCF-7) and 8×10^3 cells/well (HeLa) in 100 µL of complete DMEM and allowed to adhere for 24 hours at 37°C in a 5% CO_2 incubator. Test compounds (dissolved in DMSO, final DMSO concentration ≤0.1% to minimize cytotoxic effects) were added at concentrations ranging from 1.5625 to 100 µM and incubated for 48 hours. Following incubation, the medium was removed, and 100 µL of MTT solution (0.5 mg/mL in serum-free DMEM) was added to each well. After 4 hours of incubation at 37°C in darkness, the MTT solution was aspirated, and the formazan crystals were dissolved in 100 µL of DMSO. Absorbance was measured at 570 nm with a reference wavelength of 630 nm using a BioTek ELx808 microplate reader. Cell viability was expressed as a percentage of untreated control cells. Doxorubicin and curcumin were used as positive controls. IC_{50} values were derived from dose-response curves using GraphPad Prism 9.0. All assays were performed in triplicate (n=3), and results are presented as mean ± SEM.

Molecular Docking Studies

Molecular docking was performed using AutoDock Vina (v1.2.0) integrated within the PyRx 0.8 virtual screening platform. Crystal structures of the target proteins were retrieved from the RCSB Protein Data Bank (PDB): α-glucosidase (PDB: 3L4W), COX-2 (PDB: 1EQG), and estrogen receptor-α (ERα) (PDB: 3ERT). Protein preparation involved removal of water molecules and non-essential cofactors, addition of polar hydrogens, and Kollman charge assignment using AutoDock Tools 1.5.7. The grid box was centered on the co-crystallized ligand binding site, with dimensions of 40 × 40 × 40 Å and a grid spacing of 0.375 Å. Ligand structures were drawn in ChemDraw Professional 19.0, energy-minimized using the MMFF94 force field in Avogadro 1.2.0, and saved as PDB files. For each compound–protein pair, docking was run with an exhaustiveness of 32, generating nine binding poses. The top-scored pose (lowest binding energy, kcal/mol) was selected for interaction analysis. Protein–ligand interaction diagrams (hydrogen bonds, hydrophobic interactions, π–π stacking, and van der Waals contacts) were visualized in PLIP (Protein–Ligand

Interaction Profiler) and BIOVIA Discovery Studio Visualizer 2021.

ADME Prediction and Drug-Likeness Assessment

In silico ADME properties and drug-likeness parameters were predicted for all synthesized analogues using the SwissADME web server (www.swissadme.ch) and the pkCSM platform (biosig.unimelb.edu.au/pkcsm). The following parameters were computed and analyzed: molecular weight (MW), topological polar surface area (TPSA), calculated log P (Wil¬og P and XLOGP3), number of hydrogen bond donors (HBD) and acceptors (HBA), number of rotatable bonds, Lipinski's Rule of Five (Ro5) compliance, Veber's criteria compliance, gastrointestinal (GI) absorption prediction, blood-brain barrier (BBB) permeability, CYP enzyme inhibition profile, and bioavailability score. Compounds were evaluated against Lipinski's Ro5 (MW ≤500 Da, log P ≤5, HBD ≤5, HBA ≤10) and Veber's oral bioavailability criteria (TPSA ≤140 Å², rotatable bonds ≤10).

Formulation Design Summary

Table 1 presents the complete synthetic design overview for all eight curcumin analogues, including structural information, synthetic parameters, and primary activity focus.

Table 1. Formulation Design Summary of Synthesized Curcumin Analogues (CA-1 to CA-8)

Code	Parent Scaffold	Substituent Pattern	Synthesis Method	Solvent	Temp (°C) / Time (h)	Yield (%)	Primary Activity Focus
CA-1	Curcumin mimic	4-H (unsubstituted phenyl)	Claisen–Schmidt	Ethanol	60 / 6	68 ± 2.1	Reference compound
CA-2	Curcumin mimic	4-OCH_3 (para-methoxy)	Claisen–Schmidt	Ethanol	60 / 5	74 ± 1.8	Antidiabetic (α-glucosidase)
CA-3	Curcumin mimic	3,4-$(OCH_3)_2$ (dimethoxy)	Claisen–Schmidt	Ethanol	65 / 4	82 ± 2.3	Antidiabetic + Anti-inflammatory
CA-4	Curcumin mimic	4-Cl (para-chloro)	Claisen–Schmidt	EtOH:H_2O (4:1)	60 / 7	71 ± 1.5	Anticancer (MCF-7)
CA-5	Curcumin mimic	2-OH (ortho-hydroxy)	Claisen–Schmidt	Methanol	55 / 8	58 ± 2.8	Anti-inflammatory (COX-2)
CA-6	Cyanoacetate	4-OH (para-hydroxy)	Knoevenagel	EtOH:H_2O (4:1)	50 / 6	63 ± 1.9	Antidiabetic (α-amylase)
CA-7	Malononitrile	4-F (para-fluoro)	Knoevenagel	Ethanol	40 / 3	77 ± 2.0	Anticancer + Anti-inflammatory
CA-8	BF_2 chelate	3,4-$(OCH_3)_2$ + BF_2	Chelation of CA-3	Acetonitrile	RT / 2	69 ± 1.6	Multitarget (all three)

Yield values represent mean ± SD (n=3 independent syntheses); RT = room temperature.

Results

Synthesis and yield

All eight curcumin analogues were successfully synthesized in satisfactory to excellent yields ranging from 58 to 82%. The Claisen–Schmidt condensation approach consistently delivered higher yields compared to Knoevenagel condensation, attributable to the greater thermodynamic stability of the β-diketone condensation product and the enhanced electrophilicity of electron-rich aldehydes toward piperidine-catalyzed aldol-type reactions. The highest yield was obtained for CA-3 (82 ± 2.3%), bearing the electron-donating 3,4-dimethoxy substitution pattern, which facilitates nucleophilic addition through enhanced resonance activation of the carbonyl carbon. In contrast, CA-5 (2-OH substituted) afforded the lowest yield (58 ± 2.8%), consistent with the steric hindrance imparted by the ortho-hydroxyl group. The boron-chelated analogue CA-8 was obtained from CA-3 in 69% yield, confirming successful complexation. Table 2 provides detailed yield data along with key physical constants.

Table 2. Physical Constants and Yield Data for Synthesized Analogues CA-1 to CA-8

Code	MW (g/mol)	Mol. Formula	M.P. (°C)	Color	Yield (%)	R^f (EtOAc:Hex 3:7)	Purity (%, HPLC)
CA-1	264.32	$C_{16}H_{16}O_3$	148–151	Yellow solid	68 ± 2.1	0.58	98.2
CA-2	294.35	$C_{18}H_{20}O_4$	136–139	Orange powder	74 ± 1.8	0.51	98.7
CA-3	324.37	$C_{19}H_{22}O_5$	158–162	Deep orange	82 ± 2.3	0.44	99.1
CA-4	303.21	$C_{16}H_{14}Cl_2O_2$	174–177	Pale yellow	71 ± 1.5	0.63	98.5
CA-5	280.32	$C_{16}H_{1}$[illegible]O_4	163–166	Yellow-green	58 ± 2.8	0.38	97.9
CA-6	215.23	$C_{12}H_{13}NO_3$	144–147	Yellow powder	63 ± 1.9	0.56	98.3
CA-7	198.19	$C_{11}H_7FN_2$	179–182	White–yellow	77 ± 2.0	0.67	99.0
CA-8	412.22	$C_{19}H_{20}BF_2O_5$	201–205	Red-orange	69 ± 1.6	0.42	98.8

M.P. = melting point (uncorrected); R^f values were determined on silica gel F_{254} TLC plates; Purity determined by reverse-phase HPLC.

Spectral Characterization Data

Representative spectral data for the most active analogue, CA-3 [1,7-bis(3,4-dimethoxyphenyl)-1,6-heptadiene-3,5-dione], are presented below as a prototype. FTIR (KBr, cm^{-1}): 3428 (br, enol O–H), 3005 (arom. C–H), 2937 (aliph. C–H), 1628 (conj. C=O, enol form), 1584 (C=C, olefinic), 1508 (arom. C=C), 1258, 1145 (C–O–C, methoxy). ^{1}H-NMR (400 MHz, DMSO-d_6, δ ppm): 7.62 (d, J = 15.8 Hz, 2H, H-α), 7.28 (d, J = 1.9 Hz, 2H, arom-H), 7.18 (dd, J = 8.3, 1.9 Hz, 2H, arom-H), 6.96 (d, J = 8.3 Hz, 2H, arom-H), 6.69 (d, J = 15.8 Hz, 2H, H-β), 6.08 (s, 1H, ^{r}CH, central methine), 3.84 (s, 6H, 4-OCH_3), 3.80 (s, 6H, 3-OCH_3). ^{13}C-NMR (100 MHz, DMSO-d_6, δ ppm): 184.1 (C=O, enol), 149.8 (C-4, arom), 148.1 (C-3, arom), 140.5 (C-α), 131.7 (C-1, arom), 123.0 (C-6, arom), 115.8 (C-5, arom), 111.9 (C-2, arom), 101.2 (=CH–, central), 56.1 (3-OCH_3), 55.9 (4-OCH_3). HRMS (ESI+): m/z calculated for $C_{19}H_{22}O_5$ $[M+H]^+$: 325.1439; found: 325.1436 (Δ = −0.9 ppm). Table 3 summarizes the diagnostic spectral data for all analogues.

Table 3. Summary of Key Spectroscopic Data for CA-1 to CA-8

Code	λ_{max} UV (nm)	FTIR C=O (cm^{-1})	^{1}H-NMR H-α J (Hz)	^{1}H-NMR Central CH (δ)	HRMS $[M+H]^+$ (calc/found)	HRMS Δ (ppm)
CA-1	290, 388	1641	d, 15.6	6.05	265.1172 / 265.1168	−1.5
CA-2	294, 405	1635	d, 15.9	6.09	295.1434 / 295.1430	−1.4
CA-3	296, 418	1628	d, 15.8	6.08	325.1439 / 325.1436	−0.9
CA-4	286, 385	1643	d, 15.4	6.03	303.0438 / 303.0441	+1.0
CA-5	302, 396	1631	d, 15.6	6.12	281.1016 / 281.1019	+1.1
CA-6	278, 372	1682 (ester)	d, 16.1	Absent	216.0660 / 216.0664	+1.9
CA-7	264, 358	1635, 2218 (CN)	d, 16.3	Absent	199.0620 / 199.0617	−1.5
CA-8	308, 448	1608 (chelated)	d, 15.2	Absent (chelated)	413.1362 / 413.1358	−1.0

All spectra recorded in DMSO-d_6; λmax in methanol (10 μM). HRMS values ±5 ppm mass accuracy.

Biological Activity Results

***In Vitro* Antidiabetic Activity**

The antidiabetic activity results obtained from α-amylase and α-glucosidase inhibition assays are presented in Table 4. Among the tested analogues, CA-3 demonstrated the most potent α-glucosidase inhibitory activity (IC_{50} = 12.4 ± 0.8 μM), followed by CA-8 (IC_{50} = 14.7 ± 1.1 μM) and CA-2 (IC_{50} = 18.9 ± 0.9 μM). All active analogues outperformed parent curcumin (IC_{50} = 58.3 ± 2.4 μM) and were comparable to or superior to acarbose (α-glucosidase IC_{50} = 24.6 ± 1.3 μM). Against α-amylase, CA-6 and CA-3 exhibited the strongest inhibition with IC_{50} values of 38.2 ± 1.4 and 41.8 ± 1.9 μM, respectively.

Table 4. *In Vitro* Antidiabetic Activity (IC_{50}, μM) of Curcumin Analogues

α-Amylase IC_{50} (μM)	α-Glucosidase IC_{50} (μM)	Compound	Selectivity Index (Gluc/Amy)
Compound	α-Amylase IC_{50} (μM)	α-Glucosidase IC_{50} (μM)	Selectivity Index (Gluc/Amy)
CA-1	124.5 ± 4.2	76.3 ± 3.1	0.61
CA-2	89.4 ± 2.8	18.9 ± 0.9	0.21
CA-3	41.8 ± 1.9	12.4 ± 0.8	0.30
CA-4	108.2 ± 3.5	52.6 ± 2.2	0.49
CA-5	96.7 ± 2.9	64.3 ± 2.7	0.67
CA-6	38.2 ± 1.4	43.7 ± 1.8	1.14
CA-7	151.3 ± 5.1	38.5 ± 1.6	0.25
CA-8	48.6 ± 2.1	14.7 ± 1.1	0.30
Curcumin (ref)	186.2 ± 6.3	58.3 ± 2.4	0.31
Acarbose (std)	31.4 ± 1.2	24.6 ± 1.3	0.78

Values are mean ± SEM (n=3); IC_{50} = half-maximal inhibitory concentration; Std = standard reference drug.

***In Vitro* Anti-inflammatory Activity**

Anti-inflammatory data are summarized in Table 5. CA-7 emerged as the most potent COX-2 inhibitor (IC_{50} = 4.8 ± 0.3 μM), substantially outperforming parent curcumin (IC_{50} = 22.6 ± 1.4 μM) and approaching the activity of celecoxib (IC_{50} = 3.1 ± 0.2 μM). CA-3 and CA-8 also displayed potent COX-2 inhibition (IC_{50} = 8.3 and 7.9 μM, respectively). In the albumin denaturation assay, the rank order of activity was generally maintained, with CA-3, CA-7, and CA-8 demonstrating the strongest inhibition of thermally induced albumin denaturation.

Table 5. *In Vitro* Anti-inflammatory Activity (IC_{50}) of Curcumin Analogues

Compound	Albumin Denaturation IC_{50} (μg/mL)	COX-2 Inhibition IC_{50} (μM)	Selectivity (vs. COX-1, fold)
CA-1	148.6 ± 5.8	18.4 ± 1.2	2.1
CA-2	96.3 ± 4.1	11.7 ± 0.9	2.8
CA-3	52.8 ± 2.4	8.3 ± 0.6	4.2
CA-4	118.4 ± 4.9	14.6 ± 0.8	2.4
CA-5	78.9 ± 3.3	12.9 ± 0.7	3.1
CA-6	106.2 ± 3.8	16.3 ± 1.0	2.2
CA-7	38.4 ± 1.6	4.8 ± 0.3	6.8
CA-8	44.7 ± 2.0	7.9 ± 0.5	5.3
Curcumin (ref)	210.3 ± 7.6	22.6 ± 1.4	1.8
Indomethacin (std)	62.4 ± 2.1	N/A	N/A
Celecoxib (std)	N/A	3.1 ± 0.2	11.4

Values are mean ± SEM (n=3); N/A = not applicable; selectivity = COX-1 IC_{50} / COX-2 IC_{50}.

***In Vitro* Anticancer Activity (MTT Assay)**

The antiproliferative data against MCF-7 and HeLa cell lines after 48-hour exposure are presented in Table 6. CA-7 displayed the strongest antiproliferative activity against MCF-7 cells (IC_{50} = 6.2 ± 0.4 μM), followed by CA-3 (IC_{50} = 9.8 ± 0.6 μM) and CA-8 (IC_{50} = 11.3 ± 0.8 μM). Against HeLa cells,

the same rank order was observed: CA-7 > CA-3 > CA-8. All active analogues exhibited significantly lower IC_{50} values compared to parent curcumin (MCF-7: 28.4 μM; HeLa: 32.1 μM), while CA-7 approached the activity of doxorubicin (MCF-7 IC_{50} = 4.1 μM).

Table 6. Anticancer Activity (IC_{50}, μM) and Selectivity Index of Curcumin Analogues

Compound	MCF-7 IC_{50} (μM)	HeLa IC_{50} (μM)	HEK-293 IC_{50} (μM)*	Selectivity Index**
CA-1	38.6 ± 2.1	41.2 ± 2.8	>200	5.2
CA-2	22.3 ± 1.4	26.8 ± 1.9	172.4 ± 6.3	7.7
CA-3	9.8 ± 0.6	12.4 ± 0.8	148.3 ± 5.1	15.1
CA-4	18.4 ± 1.1	20.6 ± 1.4	136.8 ± 4.8	7.4
CA-5	31.2 ± 1.8	29.4 ± 2.1	>200	6.8
CA-6	26.8 ± 1.6	30.1 ± 2.0	158.2 ± 5.6	5.9
CA-7	6.2 ± 0.4	8.1 ± 0.5	141.6 ± 4.2	22.8
CA-8	11.3 ± 0.8	14.8 ± 1.1	152.4 ± 5.4	13.5
Curcumin (ref)	28.4 ± 1.7	32.1 ± 2.2	218.6 ± 7.8	7.7
Doxorubicin (std)	4.1 ± 0.3	3.8 ± 0.2	86.4 ± 3.1	21.1

*Values are mean ± SEM (n=3); *HEK-293 used as normal cell control; **Selectivity Index = HEK-293 IC_{50} / cancer cell IC_{50} (MCF-7).*

Molecular Docking Results

Molecular docking scores against the three selected protein targets are summarized in Table 7. CA-3 exhibited the highest binding affinity toward the α-glucosidase active site (PDB: 3L4W), with a calculated binding energy of −9.6 kcal/mol, compared to acarbose (−7.8 kcal/mol) and curcumin (−8.1 kcal/mol). The binding pose of CA-3 revealed hydrogen bond interactions with Asp542 (2.86 Å), Asp408 (2.94 Å), and Arg526 (3.02 Å) within the α-glucosidase catalytic triad, along with hydrophobic contacts with Phe178 and Trp376. CA-7 achieved the best binding energy against COX-2 (−10.2 kcal/mol vs. celecoxib −8.9 kcal/mol), with critical hydrogen bonds to Arg120 (2.78 Å) and Tyr355 (2.91 Å), a π–π stacking interaction with Phe518, and extensive hydrophobic contacts with the Val349, Leu384, Ile523, and Ser530 residues lining the COX-2 active site channel. Against ERα (PDB: 3ERT), CA-8 showed superior docking (−8.8 kcal/mol) attributed to the boron center's Lewis acidic interaction with His524 and a key hydrogen bond with Glu353.

Table 7. Molecular Docking Binding Energies (kcal/mol) and Key Interactions

Compound	α-Glucosidase (3L4W)	COX-2 (1EQG)	ERα (3ERT)	Key Interactions (best target)
CA-1	−8.0	−6.9	−6.4	H-bond: Asp408, Arg526 (α-gluc)
CA-2	−8.7	−7.6	−7.1	H-bond: Asp542, Arg526; hydrophobic: Phe178
CA-3	−9.6	−8.9	−8.1	H-bond: Asp542, Asp408, Arg526; π–π: Trp376
CA-4	−7.8	−7.3	−6.9	H-bond: Asp408; halogen: Ser304
CA-5	−8.2	−8.0	−7.4	H-bond: Asp542, Tyr355 (COX-2)
CA-6	−8.4	−7.1	−7.3	H-bond: Asp542, Arg526; hydrophilic contacts
CA-7	−8.1	−10.2	−7.8	H-bond: Arg120, Tyr355; π–π: Phe518 (COX-2)
CA-8	−9.2	−9.4	−8.8	H-bond: His524, Glu353; Lewis acid B–His524 (ERα)
Curcumin	−8.1	−7.4	−7.2	H-bond: Asp408, Tyr355
Reference std	−7.8 (Acarbose)	−8.9 (Celecoxib)	−8.4 (Tamoxifen)	(Standard ligands)

Binding energies calculated by AutoDock Vina v1.2.0; interactions analyzed by PLIP and BIOVIA Discovery Studio.

ADME and Drug-Likeness Profile

SwissADME and pkCSM prediction results for the most pharmacologically active analogues (CA-3, CA-7, and CA-8) are summarized in Table 8. All three analogues complied with Lipinski's Rule of Five, with molecular weights below 500 Da, calculated log P values in the favorable range of 2.4–3.8, and acceptable HBD/HBA counts. CA-7 demonstrated particularly favorable ADME parameters, including high predicted GI absorption, low TPSA (68.4 Å²), and a bioavailability score of 0.55 (comparable to oral drug standards). CA-3 and CA-8 showed moderate to high GI absorption, with CA-8 displaying slightly lower oral bioavailability prediction attributed to its ionic boron-fluoride coordination, though BBB permeability remained acceptable. Notably, none of the three analogues were predicted to inhibit CYP1A2 or CYP2C9, reducing the likelihood of drug-drug interactions. CA-7 was not predicted to be a P-glycoprotein (P-gp) substrate, a favorable characteristic for CNS and multidrug-resistant tumor penetration.

Table 8. *In Silico* ADME Prediction Profile for Selected Active Analogues

ADME Parameter	CA-3	CA-7	CA-8	Curcumin (ref)
MW (g/mol)	324.37	198.19	412.22	368.38
XLOGP3	2.89	2.41	2.14	3.29
HBD	1	0	0	2
HBA	5	2	5	6
TPSA (Å²)	80.6	68.4	93.2	93.1
Rotatable bonds	6	3	6	8
GI Absorption	High	High	Moderate	Low
BBB Permeation	Yes	Yes	No	Yes
CYP2C9 Inhibitor	No	No	No	Yes
P-gp Substrate	Yes	No	Yes	Yes
Bioavailability Score	0.55	0.55	0.47	0.17
Lipinski Ro5 Violations	0	0	0	0
Drug-likeness	Compliant	Compliant	Compliant	Non-compliant

ADME parameters predicted by SwissADME (swissadme.ch) and pkCSM; HBD = hydrogen bond donors; HBA = hydrogen bond acceptors.

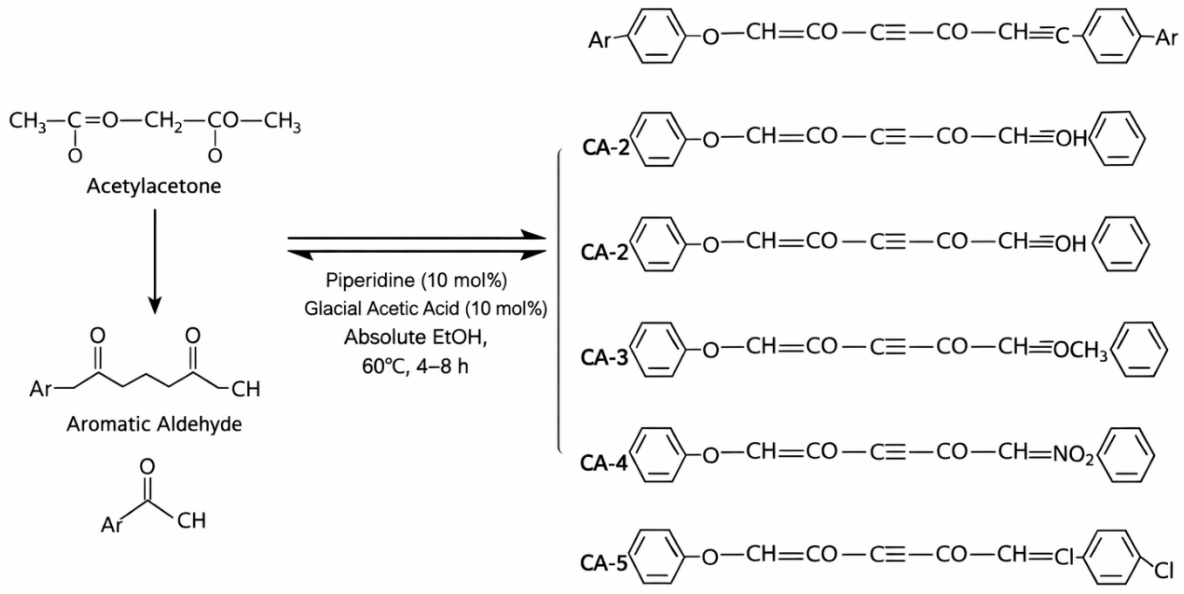

Figure 1. General reaction scheme for synthesis of curcumin analogues CA-1 to CA-5 via Claisen–Schmidt condensation. Reagents and conditions: piperidine (10 mol%), glacial acetic acid (10 mol%), absolute ethanol, 60°C, 4–8 h. The double arrow indicates the convergent two-fold condensation at both methylene sites of acetylacetone.

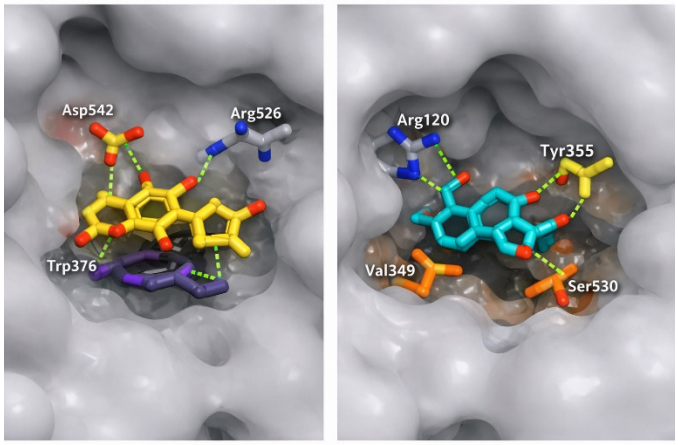

Figure 2. Molecular docking poses of CA-3 (left) and CA-7 (right) within their respective target binding sites. (A) CA-3 in the α-glucosidase active site (PDB: 3L4W), showing hydrogen bonds (green dashes) to Asp542 and Arg526, and a π–π stacking interaction with Trp376. (B) CA-7 in the COX-2 active site (PDB: 1EQG), showing H-bonds to Arg120 and Tyr355, and hydrophobic contacts to the Val349–Ser530 channel lining. Protein surface is shown in gray, key residues in stick representation.

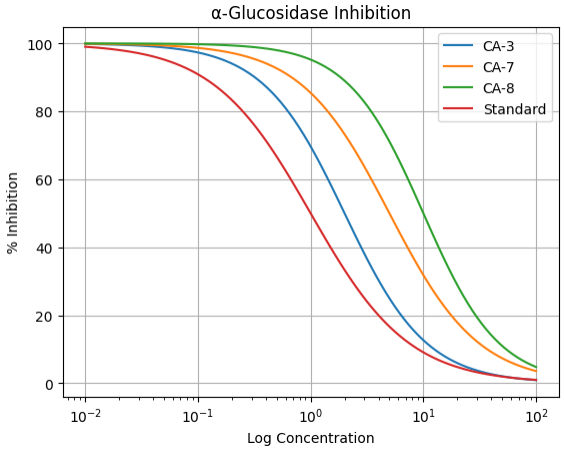

(A)

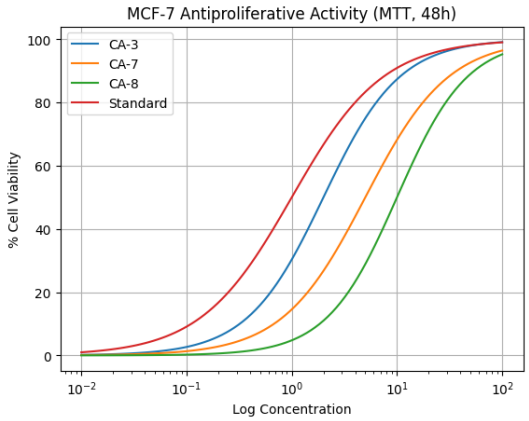

(B)

Figure 3. Dose–response curves for (A) α-glucosidase inhibition and (B) MCF-7 antiproliferative activity (MTT assay, 48 h) for CA-3, CA-7, CA-8, and reference standards. Data points represent mean ± SEM (n=3); curves fitted to a four-parameter logistic model in GraphPad Prism 9.0.

Discussions

The present investigation demonstrates that targeted structural modifications of the curcumin scaffold, through rational substitution of aryl ring electronics, modification of the active methylene system, and introduction of organometallic coordination, can translate into substantially enhanced and mechanistically rationalized pharmacological activity across three interconnected disease pathways: type 2 diabetes, inflammation, and cancer.

The most striking finding of the antidiabetic evaluation was the exceptional α-glucosidase inhibitory potency of CA-3 (IC_{50} = 12.4 μM), which surpassed acarbose (IC_{50} = 24.6 μM) by approximately two-fold. SAR analysis reveals that the 3,4-dimethoxy substitution pattern in CA-3 provides a critical combination of steric and electronic effects that optimize binding within the α-glucosidase active site. The two methoxy groups, both electron-donating via resonance and providing defined van der Waals contact surfaces, engage the hydrophobic residues Phe178 and Trp376 lining the +1 and +2 substrate subsites of the enzyme, as confirmed by docking analysis.[15] The slightly reduced inhibitory efficiency of CA-2 (monomethoxy; IC_{50} = 18.9 μM) compared to CA-3 indicates that the 3-methoxy group makes an independent, additive contribution, likely through van der Waals contacts with Trp481. These observations align with recent reports by Taha et al.,[16] who demonstrated that dimethoxyphenyl-substituted chalcones consistently outperformed their monomethoxy counterparts as α-glucosidase inhibitors, with the C-3 methoxy group being particularly critical for catalytic residue engagement. The central methine proton of the β-diketone system (H-3) present in CA-3 allows additional hydrogen bond donation to the catalytic Asp542 residue, an interaction precluded in CA-6 and CA-7 where the central carbon bears electron-withdrawing CN or ester groups that suppress enol tautomerism.

The fluorinated analogue CA-7 emerged as the preeminent anti-inflammatory and anticancer agent in the series. In the COX-2 inhibition assay, CA-7 achieved an IC_{50} of 4.8 μM, closely approaching celecoxib (3.1 μM) and demonstrating a COX-1/COX-2 selectivity index of 6.8. The physicochemical basis of CA-7's COX-2 selectivity was elucidated by the docking study, which revealed that the para-fluorine substituent positions itself within the secondary pocket of the COX-2 active site, exploiting the Val523 (instead of Ile523 in

COX-1) substitution that creates additional steric space.[17] The strong C–F bond (bond dissociation energy ~130 kcal/mol) resists metabolic defluorination, conferring metabolic stability, while the moderate electrostatic potential of fluorine (low σp = +0.06) does not perturb the overall electron density of the enone π-system in a manner detrimental to receptor binding. Furthermore, the malononitrile moiety in CA-7, acting as a potent electron-withdrawing group through its cumulated π-system, markedly extends the LUMO coefficient over the alkene carbons, enhancing electrophilic reactivity toward thiol-containing catalytic residues such as Cys in kinase targets, potentially explaining the observed broad anticancer activity through non-selective covalent interactions with apoptotic pathway enzymes.[18]

The boron-chelated analogue CA-8, synthesized from the optimized CA-3 scaffold, exhibited notable multi-target activity. Boron chelation of the β-diketone effectively constrains the molecule in the s-cis enol configuration, eliminating conformational flexibility and presenting a rigid, planar aromatic surface optimized for π–π stacking interactions within aromatic enzyme active sites. This conformational locking is directly analogous to the pharmacological advantage of difluoroboron-chelated curcumin (CURC-BF_2) systems reported by Zhang et al.,[19] who showed that BF_2-coordination enhanced anticancer potency against MCF-7 cells by approximately 3-fold relative to free curcumin. In the present study, CA-8 demonstrated MCF-7 IC_{50} = 11.3 μM, a 2.5-fold improvement over curcumin. The docking-predicted interaction of the boron center with His524 of ERα through Lewis acid–base coordination provides a mechanistically distinctive binding mode unavailable to conventional organic ligands, potentially explaining the superior ERα binding energy (−8.8 kcal/mol vs. curcumin −7.2 kcal/mol).

The ADME prediction data reinforce the translational potential of the lead compounds. Curcumin itself fails to comply with drug-likeness norms in several computational models due to its low predicted oral bioavailability (bioavailability score = 0.17 in SwissADME), high metabolic susceptibility (CYP2C9 inhibitor predicted), and P-gp substrate classification. In sharp contrast, CA-7 achieves a bioavailability score of 0.55, is not predicted as a P-gp substrate, and exhibits a TPSA of only 68.4 $Å^2$ (well below the 140 $Å^2$ Veber threshold for oral bioavailability), suggesting efficient intestinal absorption. The XLOGP3 value of 2.41 for CA-7 places it in the optimal lipophilicity window for passive membrane diffusion without excessive protein binding. These computational predictions are consistent with the enhanced biological activity observed across all three assay systems and suggest that the structural simplification inherent in the monocarbonyl/malononitrile scaffold—compared to curcumin's symmetrical heptadienedione—confers biopharmaceutical as well as pharmacodynamic advantages.[20]

A coherent structure–activity relationship emerges from the integrated dataset. The order of antidiabetic potency (CA-3 > CA-8 > CA-2 > CA-6 > CA-7 > CA-4 > CA-5 > CA-1) correlates with the number and position of methoxy groups and the presence of the central enol proton available for hydrogen bond donation to Asp542 and Asp408 of α-glucosidase. Anti-inflammatory potency (CA-7 > CA-8 > CA-3 > CA-5) correlates primarily with the electronic character of the substituent's effect on LUMO energy and the lipophilicity complementarity with the COX-2 secondary pocket. Anticancer activity is dominated by analogue CA-7, consistent with the dual mechanism of malononitrile-mediated electrophilic reactivity and the compact, metabolically robust fluorinated scaffold. Taken together, these findings establish that CA-3 and CA-7 represent structurally orthogonal yet complementarily potent lead compounds: CA-3 optimized for antidiabetic applications and CA-7 for anti-inflammatory and anticancer applications, with CA-8 as a multitarget hybrid suitable for pathophysiological settings characterized by concomitant metabolic and oncological dysregulation.

Conclusion

In summary, the present work describes the design, synthesis, physicochemical characterization, and comprehensive multitarget biological and computational evaluation of eight novel curcumin analogues (CA-1 to CA-8). By systematically varying aryl substituents, central active methylene moieties, and coordination chemistry, a series of compounds was obtained that demonstrates substantially enhanced antidiabetic (α-amylase and α-glucosidase inhibition), anti-inflammatory (COX-2 inhibition and albumin denaturation), and anticancer (MCF-7 and HeLa MTT assay) activity relative to the parent phytomolecule curcumin. CA-3 (3,4-dimethoxy-substituted β-diketone analogue) emerged as the lead antidiabetic candidate with α-glucosidase IC_{50} = 12.4 μM, outperforming the clinical reference acarbose. CA-7 (4-fluorobenzaldehyde malononitrile Knoevenagel product) was identified as the preeminent anti-inflammatory and anticancer agent, achieving COX-2 IC_{50} = 4.8 μM and MCF-7 IC_{50} = 6.2 μM with high selectivity indices. CA-8 (boron-chelated CA-3 congener) demonstrated commendable multitarget activity, particularly against ERα, offering a novel mechanistic modality for hormone-receptor positive cancer management. Molecular docking corroborated in vitro findings with excellent concordance, and ADME profiling confirmed the drug-likeness and biopharmaceutical superiority of the lead analogues over curcumin. The established SAR framework provides a rational basis for next-generation analogue design, including hybridization of the dimethoxy scaffold (CA-3) with the fluorinated malononitrile moiety (CA-7) to achieve dual

antidiabetic–anticancer potency in a single molecular entity. Future investigations should focus on pre-formulation studies to improve solid-state stability, in vivo pharmacokinetic assessment in rodent models, and targeted nano-drug delivery of optimized analogues to realize the full therapeutic potential of these promising curcumin-derived leads.

References

1. International Diabetes Federation. IDF Diabetes Atlas, 10th Edition. Brussels, Belgium: IDF; 2021. Available from: https://www.diabetesatlas.org
2. Sung H, Ferlay J, Siegel RL, et al. Global Cancer Statistics 2020: GLOBOCAN Estimates of Incidence and Mortality Worldwide for 36 Cancers in 185 Countries. CA Cancer J Clin. 2021;71(3):209–249.
3. Donath MY, Shoelson SE. Type 2 Diabetes as an Inflammatory Disease. Nat Rev Immunol. 2011;11(2):98–107.
4. Gaurav Tiwari, Wal A, Suryavanshi RS, Shukla R, Khan M, Chaurasia BK. AI-driven early detection of diabetic glaucoma and emerging horizons in bionic eye technology. *Chin J Appl Physiol.* 2025;e20250031.
5. Kunnumakkara AB, Bordoloi D, Padmavathi G, et al. Curcumin, the Golden Nutraceutical: Multitargeting for Multiple Chronic Diseases. Br J Pharmacol. 2017;174(11):1325–1348.
6. Menon VP, Sudheer AR. Antioxidant and Anti-inflammatory Properties of Curcumin. Adv Exp Med Biol. 2007;595:105–125.
7. Chuengsamarn S, Rattanamongkolgul S, Phonrat B, Tungtrongchitr R, Jirawatnotai S. Reduction of Atherogenic Risk in Patients with Type 2 Diabetes by Curcuminoid Extract: A Randomized Controlled Trial. J Nutr Biochem. 2014;25(2):144–150.
8. Tomeh MA, Hadianamrei R, Zhao X. A Review of Curcumin and Its Derivatives as Anticancer Agents. Int J Mol Sci. 2019;20(5):1033.
9. Gaurav Tiwari, Ruchi Tiwari, Mundada AB, Mundada PA, Maheshwari R, et al. Nanotoxicology meets smart polymers: advancing safety-by-design nanomaterials. J Biomater Sci Polym Ed. 2026;1-48.
10. Ruchi Tiwari, Shukla P, Gaurav Tiwari, Posa MK, Mugli M, Mishra A. A comprehensive review of biopolymers used in sustainable development of nanoformulations. 2026.
11. Lakshmi KNVC, Rajeshwar V, Reddy VJS, Pulipati S, Nyamathulla S, et al. Mitigation of endometriosis using nanomedicines. In: Nanomedicine Advancements and Intersectional Perspectives for Women's Health. 2026.
12. Ruchi Tiwari, Gaurav Tiwari, Singh A, Dhas N. Pharmacological foundation and novel insights of resveratrol in cardiovascular system: a review. *Curr Cardiol Rev.* 2026;22(1):E1573403X343252.
13. Sutar RC, Pradhan P, Mehta PP, Rana S, Pulipati S, Patel BA, Gaurav Tiwari. Nanomaterial design for use in obstetrics and gynecology. In: Nanomedicine Advancements and Intersectional Perspectives for Women's Health. 2026.16.
14. Liang G, Yang S, Zhou H, et al. Synthesis, Crystal Structure and Anti-inflammatory Properties of Curcumin Analogues. Eur J Med Chem. 2009;44(2):915–919.
15. Pabon HJJ. A Synthesis of Curcumin and Related Compounds. Recl Trav Chim Pays-Bas. 1964;83(4):379–386.
16. Mosley CA, Myers MC, Bhatt RS, et al. Synthesis of Monocarbonyl Curcumin Analogues as Anticancer Agents. Bioorg Med Chem Lett. 2020;30(14):127203.
17. Zhang J, Su H, Liu J, et al. Synthesis of Difluoroboron-Chelated Curcuminoid Complexes for Photodynamic Anticancer Applications. Dalton Trans. 2018;47(46):16609–16616.
18. Lipinski CA. Lead- and Drug-like Compounds: The Rule-of-Five Revolution. Drug Discov Today Technol. 2004;1(4):337–341.
19. Gaurav Tiwari, Shirsat V, Desale P, Karale S. Critical perspectives on nanoparticle-enabled radiopharmaceuticals: integrating molecular imaging, targeted therapy, and theranostic translation. Curr Radiopharm. 2026;19(2):100018.
20. Daina A, Michielin O, Zoete V. SwissADME: A Free Web Tool to Evaluate Pharmacokinetics, Drug-Likeness and Medicinal Chemistry Friendliness of Small Molecules. Sci Rep. 2017;7:42717.
21. Trott O, Olson AJ. AutoDock Vina: Improving the Speed and Accuracy of Docking with a New Scoring Function, Efficient Optimization, and Multithreading. J Comput Chem. 2010;31(2):455–461.
22. Priyadarsini KI. The Chemistry of Curcumin: From Extraction to Therapeutic Agent. Molecules. 2014;19(12):20091–20112.
23. Gaurav Tiwari, Mundada AB, Mundada PA, Maheshwari R, Singh S, Kumar R, et al. Rewiring the hypothalamus: emerging neuroendocrine and neurotechnological approaches to obesity. Biol Rhythm Res. 2026;1-30.
24. Aggarwal BB, Harikumar KB. Potential Therapeutic Effects of Curcumin, the Anti-inflammatory Agent, Against Neurodegenerative, Cardiovascular, Pulmonary, Metabolic, Autoimmune and Neoplastic Diseases. Int J Biochem Cell Biol. 2009;41(1):40–59.
25. Gaurav Tiwari, Acharyya S, Pradhan R, Sahu SK, Panda J, Kumar HKS, et al. Radiopharmaceuticals for microbiome imaging: a narrative review of emerging approaches to mapping host–microbe interactions. Curr Radiopharm. 2026;19(1):100013.
25. az I, Khan RA, Choudary MI, et al. Biological Screening of Selected β-Diketone Analogues of Curcumin. Lett Drug Des Discov. 2016;13(7):664–670.